IOP Publishing Journal of Physics: Condensed Matter
J. Phys.: Condens. Matter **32** (2020) 265701 (8pp) https://doi.org/10.1088/1361-648X/ab7a4c

Drift velocity saturation and large current density in intrinsic three-dimensional Dirac semimetal cadmium arsenide

S S Kubakaddi

Department of Physics, K. L. E. Technological University, Hubballi-580031, Karnataka, India

E-mail: sskubakaddi@gmail.com

Received 27 November 2019, revised 7 February 2020
Accepted for publication 26 February 2020
Published 31 March 2020

Abstract

Transport of electrons at high electric fields is investigated in intrinsic three-dimensional Dirac semimetal cadmium arsenide, considering the scattering of electrons from acoustic and optical phonons. Screening and hot phonon effect are taken in to account. Expressions for the hot electron mobility μ and power loss P are obtained as a function of electron temperature T_e. The dependence of drift velocity v_d on electric field E and electron density n_e has been studied. Hot phonon effect is found to set in the saturation of v_d at relatively low E and to significantly degrade its magnitude. The drift velocity is found to saturate at a value $v_{ds} \sim 10^7$ cm s^{-1} and it is weakly dependent on n_e. A large saturation current density $\sim 10^6$ A cm^{-2} is predicted.

Keywords: three-dimensional Dirac semimetal, electron–phonon interaction, drift velocity and current density saturation

1. Introduction

Three-dimensional Dirac semimetal (3DDS) cadmium arsenide, a 3D analog of graphene, is one of the most emergent class of materials in current condensed matter physics (for review see references [1, 2]). Interest in the study of electronic properties of 3DDS cadmium arsenide (Cd_3As_2) was initiated by its theoretical prediction [3], and experimental realization [4–8]. The linear band dispersion with gapless feature has led massless Dirac fermions in this material to exhibit many unusual transport phenomena such as quantum oscillations [9, 10], ultrahigh mobility [8, 10, 11] and giant magnetoresistance [8, 11, 12]. Moreover, recently quantum Hall effect has been observed in films of Dirac semimetal Cd_3As_2 [13, 14].

Very large mobilities $> \sim 10^7$ cm^2 V^{-1} s^{-1} have been reported in 3DDS Cd_3As_2 at low-temperature ~ 5 K [8, 10]. Resistivity measurements as a function of temperature T have shown metallic behavior with the residual resistivity as low as 11.6 nΩ cm at $T < 6$ K [10]. Such ultra-large (small) mobilities (resistivities) are attributed to the suppressed back scattering of high-velocity massless Dirac fermions. In a sample with impurities, the residual mobility has been found to be $\sim 2 \times 10^5$ cm^2 V^{-1} s^{-1} at $T \sim 2.6$ K and it decreases with increasing temperature, reaching finally a value of $\sim 2 \times 10^4$ cm^2 V^{-1} s^{-1} at room temperature [15]. Some recent experiments have also shown room temperature mobility $> \sim 10^4$ cm^2 V^{-1} s^{-1} [16, 17]. In addition, in 3DDS Cd_3As_2, the electron density n_e is ultra-large ($\sim 10^{18}$ to 10^{20} cm^{-3}) [7, 15, 18, 19], exceeding the electron densities in traditional semiconductors. The behavior of temperature dependence of the resistivity/mobility was inferred to be due to the impurity scattering at low-temperature and phonon scattering at higher temperature.

There have been a few theoretical investigations of the transport properties in 3DDS Cd_3As_2, that consider the scattering by short-range disorder and charged impurities, using the Boltzmann transport equation [20, 21]. Very recently, we have given a theory of the phonon-limited mobility of high density Dirac fermions in 3DDS Cd_3As_2 considering the electron scattering by acoustic and optical phonons in the quasi-elastic approximation [22]. Experimental results of the mobility have been quantitatively explained by applying this theory.

The above mentioned transport studies have been made in the low electric field. In the high electric field, hot electron cooling as a function of electron temperature has been theoretically investigated [23–25]. However, there have been no reports, either experimentally or theoretically, giving the electron drift velocity v_d dependence of electric field E in the high field region where v_d tends to saturate. In the Drude model, the current density is given by $j = n_e e v_d$. Realization and control of saturation drift velocity v_{ds}/current density j_s is an important design measure for the device applications of field effect transistors (FETs) at high electric field. FETs for analog and radiofrequency (RF) applications ideally operate in the saturation limit. By virtue of the excellent carrier mobility at room temperature and large n_e, the 3DDS Cd_3As_2 is expected to give rise to a large saturation current density. Thus, Cd_3As_2 can be considered as a potential candidate in high efficiency RF and analog devices.

Very recently, the two-dimensional Dirac fermions have been realized in films of Cd_3As_2 [13, 26, 27]. FETs using Cd_3As_2 film of thickness 30 nm as the channel material are demonstrated [27]. These FETs have shown extremely high current densities and low contact resistances and are very promising for future high-speed electronics and RF applications.

In view of the above observations, an understanding of the velocity-field characteristics in 3DDS Cd_3As_2 is very essential. These characteristics have been extensively studied in bulk semiconductors [28–30], low-dimensional semiconductors [31] and graphene [32–37]. In the present work we have conducted a study of drift velocity and current density behavior as a function of electric field and electron density in 3DDS Cd_3As_2. The hot electron mobility and energy balance equations are employed to explore this behavior. Since the nearly intrinsic samples have been realized for $T > \sim 5$ K [8, 10], we have considered phonons as the only scattering channel.

The theory of hot electron intrinsic mobility is developed for the first time in 3DDS by including the hot phonon effect and screening. It is presented, along with the hot electron power loss equations, in section 2. Using these equations, the velocity-field curves are obtained by numerical solution. The results and discussion are presented in section 3. Finally, our findings are summarised in section 4.

2. Analytical model for high field transport in three-dimensional Dirac semimetal

We consider Dirac fermions in a disorder free 3DDS Cd_3As_2 with a large electron density so that the Fermi energy E_F is well above the Dirac points. The electron energy dispersion is linear, i.e., $E_{\mathbf{k}} = \hbar v_F k$, and the density of states is $D(E_{\mathbf{k}}) = g E_{\mathbf{k}}^2/[2\pi^2(\hbar v_F)^3]$, where v_F is the Fermi velocity, $\mathbf{k}$ is the 3D wave vector, and $g = g_s g_v$, with g_s (g_v) denoting the spin (valley) degeneracy of the electron. We assume that the electronic dispersion is isotropic [4, 21–23], although it has been found by some authors to be anisotropic [3, 7, 8]. In an applied electric field E, electrons gain energy and momentum, and, in the steady state, they establish their electron temperature T_e ($>T$, the lattice temperature) and drift velocity v_d, by losing extra energy and momentum to the lattice (phonons). The electrons are assumed to obey the hot-electron Fermi–Dirac (F–D) distribution $f_o(E_{\mathbf{k}}) = \{\exp[(E_{\mathbf{k}} - E_F)/k_B T_e] + 1\}^{-1}$. The three parameters T_e, v_d and the hot electron mobility $\mu = v_d/E$ give a full description of the 3D Dirac electrons in non-equilibrium.

We assume that electrons interact with the intrinsic acoustic phonons (ap) and optical phonons (op). Since we consider a Cd_3As_2 with large $n_e \sim (10^{18}$ to 10^{20} cm$^{-3})$, the electron scattering by both ap and op is assumed to be quasi-elastic, noting that the optical phonon energy ~ 25 meV [38] is considerably smaller than the E_F. Hence, we can obtain the phonon-limited hot electron intrinsic mobility μ using the semi-classical Boltzmann transport equation solved in the relaxation time approximation. The mobility, thus obtained, will be a function of T_e. In the steady state, the energy balance equation is given by $eEv_d = P$, where eEv_d is the power gained by electron from the field E and $P = \langle dE_{\mathbf{k}}/dt\rangle_{el-ph}$ is the power loss per electron to the lattice by electron–phonon (el–ph) interaction. P can be calculated by the standard technique [25, 28] and it is a function of T_e. Combining the equation for drift velocity $v_d = \mu E$ and $eEv_d = P$, an expression relating T_e to E can be obtained. Hence, v_d vs E curves are deduced.

2.1. Phonon-limited hot electron mobility μ

From the Boltzmann transport equation technique, using the relaxation time approximation, an expression for the mobility is given by [22]

$$\mu_i = \sigma_i/n_e e, \tag{1}$$

with electrical conductivity $\sigma_i = e^2 K_{0i}$, where

$$K_{0i} = \frac{v_F^2}{3}\int dE_{\mathbf{k}} D(E_{\mathbf{k}})\tau_i(E_{\mathbf{k}})\left(-\frac{\partial f_o(E_{\mathbf{k}})}{\partial E_{\mathbf{k}}}\right), \tag{1a}$$

and $i =$ ap and op. For $E_F \gg k_B T_e$, expression for the mobility takes the simple form $\mu_i = [ev_F{}^2 D(E_F)\tau_i(E_F)]/3n_e$.

Considering the electron interaction with the intrinsic phonons of energy $\hbar\omega_{\mathbf{q}}$ and wave vector $\mathbf{q}$, the energy-dependent hot electron momentum relaxation time $\tau(E_{\mathbf{k}})$ for the scattering due to phonons, following reference [22], is shown to be

$$\frac{1}{\tau(E_{\mathbf{k}})} = \left(\frac{V}{2\pi\hbar(\hbar v_F)^3}\right)[1 - f_o(E_{\mathbf{k}})]^{-1}\int_0^{\pi} d\theta\,(1-\cos\theta)] \times \sin\theta\frac{|C(q)|^2}{\varepsilon^2(q)}\left\{N_{\mathbf{q}}\left(E_{\mathbf{k}}+\hbar\omega_{\mathbf{q}}\right)^2\left[1 - f_o\left(E_{\mathbf{k}}+\hbar\omega_{\mathbf{q}}\right)\right] + \left(N_{\mathbf{q}}+1\right)\left(E_{\mathbf{k}}-\hbar\omega_{\mathbf{q}}\right)^2\left[1 - f_o(E_{\mathbf{k}}-\hbar\omega_{\mathbf{q}})\right]\theta(x)\right\}, \tag{2}$$

where V is the volume of the crystal, θ is the angle between the initial state $\mathbf{k}$ and final state $\mathbf{k}'$, $|C(q)|^2$ is the electron–phonon matrix element, $\varepsilon(q)$ is the screening function, $N_{\mathbf{q}}$ is the phonon distribution function, and $\theta(x)$ is the step function with $x = (E_{\mathbf{k}} - \hbar\omega_{\mathbf{q}})$. We take the temperature independent screening function $\varepsilon(q) = [1 + (q_{TF}/q)^2]$ in the Thomas–Fermi

approximation, where $q_{TF} = [4\pi e^2 D(E_F)/\varepsilon_s]^{1/2}$ is the Thomas–Fermi wave vector [21]. This is valid for $T_e \ll T_F$, where T_F is the Fermi temperature. In the following, we obtain the hot electron momentum relaxation time due to the scattering by acoustic and optical phonons.

2.1.1. Hot electron momentum relaxation time due to acoustic phonon scattering. The electron scattering by the longitudinal acoustic phonons is taken to be via deformation potential coupling. The corresponding interaction matrix element is given by $|C(q)|^2 = [(D^2\hbar\omega_{\mathbf{q}})/(2\rho_m V v_s{}^2)](1+\cos\theta)/2$ [21, 23], where D is the acoustic deformation potential constant, ρ_m is the mass density, $\omega_{\mathbf{q}} = v_s q$, and v_s is the velocity of acoustic phonon. Assuming the acoustic phonons to be in thermal equilibrium with the lattice, $N_{\mathbf{q}}$ is given by the Bose distribution $N_{\mathbf{q}}(T) = \{\exp[(\hbar\omega_{\mathbf{q}})/k_B T] - 1\}^{-1}$ at lattice temperature T. Using the quasi-elastic approximation, the relaxation time $\tau_{ap}(E_{\mathbf{k}})$ for the acoustic phonon scattering is given by

$$\frac{1}{\tau_{ap}(E_{\mathbf{k}})} = \frac{D^2 v_F}{8\pi\rho_m v_s^2(\hbar v_s)^4 E_{\mathbf{k}}^2(k_B T_e)}\int_0^{2\hbar v_s k} \mathrm{d}(\hbar\omega_{\mathbf{q}})\frac{(\hbar\omega_{\mathbf{q}})^5}{\varepsilon^2(q)} \times\left[1-\left(\frac{\hbar\omega_{\mathbf{q}}}{E_{\mathbf{k}}}\right)^2\left(\frac{v_F}{2v_s}\right)^2\right][N_{\mathbf{q}}(T)+1]N_{\mathbf{q}}(T_e) \times\left\{\exp\left[\left(\frac{\hbar\omega_{\mathbf{q}}}{k_B}\right)\left(\frac{1}{T_e}-\frac{1}{T}\right)\right]+1\right\}. \quad (3)$$

We obtain the simple analytical forms of $\tau_{ap}(E_{\mathbf{k}})$ in special cases of very low temperature i.e. Bloch–Grüneisen (BG) regime, $T \ll T_{BG}$, and high temperature i.e. equipartition (EP) regime, $T > T_{BG}$. The Bloch–Grüneisen temperature T_{BG} is defined by $k_B T_{BG} = 2\hbar v_s k_F$, where k_F is the Fermi wave vector.

(a) *Very low temperature*: in the BG regime, $q \to 0$ as $T \to 0$, $\hbar\omega_{\mathbf{q}} \approx k_B T$, and $\hbar\omega_{\mathbf{q}} \ll k_B T_e$. We set $k = k_F$ (the Fermi wave vector), $E_{\mathbf{k}} = E_F$ and $\varepsilon(q) \approx (q_{TF}/q)^2$. Then, the momentum relaxation time in the BG regime is given by

$$\frac{1}{\tau_{ap-BG}(E_{\mathbf{F}})} = \frac{9!D^2(hv_F)}{8\pi\rho_m v_s(\hbar v_s)^5 E_F^2(\hbar v_s q_{TF})^4} \times\left[\frac{(k_B T_e)^{10}+(k_B T)^{10}}{k_B T_e}\right] \quad (4a)$$

with screening, and

$$\frac{1}{\tau_{ap-BG}(E_{\mathbf{F}})} = \frac{15D^2(hv_F)}{\pi\rho_m v_s(\hbar v_s)^5 E_F^2}\left[\frac{(k_B T_e)^6+(k_B T)^6}{k_B T_e}\right] \quad (4b)$$

without screening.

Thus, in 3DDS, for $T_e \gg T$, we find that

$$\tau_{ap-BG}(E_F) \sim T_e^{-9} \text{ and } T_e^{-5}, \quad (4c)$$

respectively, for the screened and unscreened el–ph interaction. This T_e dependence is same as in the conventional degenerate 3D semiconductor [39] and it is manifestation of the 3D nature of acoustic phonons, noting that screening is taken to be independent of temperature. Correspondingly, the acoustic phonon limited BG regime hot electron mobility gives the following T_e dependence

$$\mu_{ap-BG} \sim T_e^{-9}\left(T_e^{-5}\right), \text{ with (without) screening.} \quad (4d)$$

It is to be noted that for the low field case, $T_e = T$, and equations (4a)–(4d) reduce to those in reference [22]. We also find that n_e dependence of hot electron $\mu_{ap\text{-}BG}$ is given by

$$\mu_{ap-BG} \sim n_e^{5/3}\left(n_e^{1/3}\right), \text{ with (without) screening.} \quad (4e)$$

It is the same as found for low field case in reference [22].

(b) *High temperature*: in the EP regime, $\hbar\omega_{\mathbf{q}} \ll k_B T, k_B T_e$, equation (3) simplifies to

$$\frac{1}{\tau_{ap-EP}(E_{\mathbf{k}})} = \frac{D^2 v_F(k_B T)}{8\pi\rho_m v_s^2(\hbar v_s)^4 E_{\mathbf{k}}^2}\int_0^{2\hbar v_s k} \mathrm{d}(\hbar\omega_{\mathbf{q}})\frac{(\hbar\omega_{\mathbf{q}})^3}{\varepsilon^2(q)} \times\left[1-\left(\frac{\hbar\omega_{\mathbf{q}}}{E_{\mathbf{k}}}\right)^2\left(\frac{v_F}{2v_s}\right)^2\right] \times\left[2+\frac{\hbar\omega_{\mathbf{q}}}{k_B}\left(\frac{1}{T_e}-\frac{1}{T}\right)\right]. \quad (5a)$$

For unscreened el–ap coupling, it may be approximated to give a simple form

$$\frac{1}{\tau_{ap-EP}(E_{\mathbf{k}})} = \frac{D^2 v_F(k_B T)E_{\mathbf{k}}^2}{3\pi\rho_m v_s^2(\hbar v_s)^4} \quad (5b)$$

which is independent of T_e. Interestingly, in the EP regime, for $E_k = E_F$, the $\tau_{ap\text{-}EP}(E_F)$ and the corresponding mobility $\mu_{ap\text{-}EP}$ are the same as in the low field case [22]. Consequently, T and n_e dependence of $\mu_{ap\text{-}EP}$ are also same as that found for zero field case i.e.

$$\mu_{ap-EP} \sim T^{-1} \text{ and } n_e^{-1}. \quad (5c)$$

2.1.2. Hot electron momentum relaxation time due to optical phonon scattering. We consider the electron–polar optical phonon interaction via Fröhlich interaction and the corresponding matrix element is given by $|C(q)|^2 = (C_0/q^2)(1+\cos\theta)/2$, where $C_0 = (2\pi e^2\hbar\omega_0\varepsilon')/V$, $\hbar\omega_q = \hbar\omega_0$ is the optical phonon energy, $\varepsilon' = (\varepsilon_\infty{}^{-1} - \varepsilon_s{}^{-1})$, and ε_∞ (ε_s) is the high-frequency (static) dielectric constant. In high electric field, the optical phonon distribution will deviate from its thermal equilibrium value $N_{\mathbf{q}}(T)$ and it is given by the hot phonon distribution function $N_{\mathbf{q}hp}$ [25]. Assuming the scattering to be quasi-elastic, the momentum relaxation time due to optical phonons, taking account of the hot phonon effect and screening, is found to be

$$\frac{1}{\tau_{\rm op}(E_{\mathbf{k}})} = \frac{e^2\hbar\omega_0\varepsilon'}{2\hbar^2 v_{\rm F}}\left(\frac{\hbar\omega_0}{k_{\rm B}T_{\rm e}}\right)\int_0^{\pi} {\rm d}\theta\,\sin\theta\left(\frac{1+\cos\theta}{2}\right) \times \left\{\begin{array}{l} \dfrac{N_{\mathbf{q}_+\mathbf{ph}}[N_{\mathbf{q}}(T_{\rm e})+1]\,\left(1+(\hbar\omega_0/E_{\mathbf{k}})\right]}{\varepsilon^2(q_+)} \\ +\dfrac{[N_{\mathbf{q}_-\mathbf{ph}}+1]N_{\mathbf{q}}(T_{\rm e})[1-\left(\hbar\omega_0/E_{\mathbf{k}}\right]\theta(x)}{\varepsilon^2(q_-)} \end{array}\right\}, \tag{6}$$

where

$$q_+^2 = (1/\hbar v_{\rm F})^2\left[2E_{\mathbf{k}}^2 + 2E_{\mathbf{k}}\hbar\omega_o + (\hbar\omega_o)^2 - 2E_{\mathbf{k}}(E_{\mathbf{k}}+\hbar\omega_o)\cos\theta\right] \tag{6a}$$

and

$$q_-^2 = (1/\hbar v_{\rm F})^2\left[2E_{\mathbf{k}}^2 - 2E_{\mathbf{k}}\hbar\omega_o + (\hbar\omega_o)^2 - 2E_{\mathbf{k}}(E_{\mathbf{k}}-\hbar\omega_o)\cos\theta\right]. \tag{6b}$$

In equation (6), $N_{\mathbf{q}_+\rm ph}$ and $N_{\mathbf{q}_-\rm ph}$ are the hot phonon distribution functions with $q = q_+$ and $q = q_-$, respectively, considering the screening of el–op interaction.

The hot electron mobility due to ap and op scattering can be obtained by using the respective relaxation times (i.e. equations (3) and (6)) in equation (1). The resultant phonon-limited hot electron mobility is given by $\mu = [(1/\mu_{\rm ap}) + (1/\mu_{\rm op})]^{-1}$.

From the equation $v_{\rm d} = \mu E$, the momentum balance equation can be obtained as $eE = (ev_{\rm d}/\mu) = Q$, where eE is the force on an electron due to electric field E. The substitution of phonon-limited hot electron mobility μ, on rhs, gives the momentum loss rate Q due to phonons. Conventionally, Q is obtained by finding the average momentum loss rate $\langle {\rm d}\hbar\mathbf{k}/{\rm d}t\rangle$ to the lattice using the displaced hot electron F–D distribution [28, 40, 41].

2.2. Hot electron power loss P

The hot electron power loss due to the intrinsic acoustic and optical phonons has been investigated by us in detail [24, 25]. For the of sake completeness, their final results are given here. The power loss due to acoustic phonons, with screened el–ap interaction, is given by

$$P_{\rm ap} = -\frac{gD^2}{8\pi^3\rho\hbar^7 n_{\rm e} v_{\rm F}^4 v_{\rm s}^4}\int_0^{\infty} {\rm d}E_{\mathbf{k}}\int_0^{(\hbar\omega_q)_{\max}} {\rm d}(\hbar\omega_{\mathbf{q}})(\hbar\omega_{\mathbf{q}})^3 \times \frac{(E_{\mathbf{k}}+\hbar\omega_{\mathbf{q}})^2}{\varepsilon^2(q)}|F(E_{\mathbf{k}},E_{\mathbf{q}})|^2[N_{\mathbf{q}}(T_{\rm e}) - N_{\mathbf{q}}(T)] \times [f_0(E_{\mathbf{k}}) - f_0(E_{\mathbf{k}}+\hbar\omega_{\mathbf{q}})]. \tag{7}$$

Taking account of the hot phonon effect and screening of el–op interaction, the power loss due to optical phonons is shown to be

$$P_{\rm op} = \frac{g(\hbar\omega_0)^2 e^2\varepsilon'}{2\pi^2\hbar n_{\rm e}(\hbar v_{\rm F})^4}\int_0^{\infty} {\rm d}E_{\mathbf{k}}E_{\mathbf{k}}\int_0^{E_{\mathbf{q}u}} {\rm d}E_{\mathbf{q}}\frac{|F(E_{\mathbf{k}},E_{\mathbf{q}})|^2}{E_{\mathbf{q}}\varepsilon^2(q)} \times [(N_{\mathbf{q}\rm hp}+1)\,{\rm e}^{-(\hbar\omega_0/k_{\rm B}T_{\rm e})} - N_{\mathbf{q}\rm hp}] \times f_0(E_{\mathbf{k}})[1-f_0(E_{\mathbf{k}}+\hbar\omega_0)]\,|E_{\mathbf{k}}+\hbar\omega_0|\,, \tag{8}$$

where

$$|F(E_{\mathbf{k}},E_{\mathbf{q}})|^2 = (1/2)\{1+[(E_{\mathbf{k}}{}^2 - E_{\mathbf{q}}{}^2) + (E_{\mathbf{k}}+\hbar\omega_0)^2] \times [2E_{\mathbf{k}}(E_{\mathbf{k}}+\hbar\omega_0)]^{-1}\} \tag{8a}$$

and $E_{\mathbf{q}u} = (2E_{\mathbf{k}} + \hbar\omega_0)/2$. The equation (8) is obtained from our work [25] by combining equations (16) and (6) (in reference [25]) and substituting for $|g(q)|^2 = [(2\pi e^2\hbar\omega_0\varepsilon')/Vq^2]$.The total power loss is given by $P = P_{\rm ap} + P_{\rm op}$. The energy balance equation is obtained as $eEv_{\rm d} = P$.

It should be noted that the method adopted here to obtain $v_{\rm d}$ as a function of E is analytical, unlike other numerical methods [29, 32, 36, 37].

3. Results and discussion

In the previous section, the expressions for the hot electron mobility μ (hence for the drift velocity $v_{\rm d}$) and the energy balance form the two transcendental equations. We numerically solve these coupled equations for a chosen $T_{\rm e}$ to obtain velocity-field curves for the 3DDS Cd_3As_2. The material parameters used are: $v_{\rm F} = 1\times10^8$ cm s^{-1} [21–23, 42], $v_{\rm s} = 2.3\times10^5$ cm s^{-1}, $\rho_{\rm m} = 7.0$ g cm^{-3}, $\varepsilon_\infty = 12$, $\varepsilon_{\rm s} = 36$, and $g = 4$. A reasonable value of $D = 20$ eV [22, 43] and a typical value of $\hbar\omega_0 = 25$ meV [22, 38] are chosen. Throughout the discussion, $n_0 = 1\times10^{18}$ cm^{-3} is used. We note that in the nearly intrinsic experimental samples $n_{\rm e} \sim 1$–$10n_0$ [8, 10]. The reasonable values of hot phonon relaxation time $\tau_{\rm p} = 1$ and 5 ps are used in the demonstration. These values of $\tau_{\rm p}$ are of the order which have been experimentally shown [44] and used in theoretical calculations [37, 45] for graphene. Also, in III–V semiconductors $\tau_{\rm p}$ is of the order of a few ps [40].

In order to analyze the $v_{\rm d}$ vs E characteristics, we need to understand the $T_{\rm e}$ dependence on E, because P and μ are determined by $T_{\rm e}$. A representative $T_{\rm e}$ vs E behavior is depicted in figure 1(a) for $n_{\rm e} = n_0$ and $5n_0$, $T = 4.2$ K and $\tau_{\rm p} = 0$ ps. It has been found that, with increasing E, $T_{\rm e}$ deviates from T and sets increasing rapidly at about $E = 0.03$ (0.1) V cm^{-1} for $n_{\rm e} = n_0$ ($5n_0$). In this low field region electrons dissipate their energy by emission of acoustic phonons whose energy is much less than the electron energy and $T_{\rm e}$ keeps increasing with electric field E. For $E > \sim$0.2 and 0.6 V cm^{-1}, respectively, for $n_{\rm e} = n_0$ and $5n_0$, the rate of increase of $T_{\rm e}$ slows down. This is the region where electron–optical phonon scattering plays the dominant role as an energy dissipation channel. At still higher fields ($E > \sim$0.1 kV cm^{-1}), even emission of optical phonons may be less effective in limiting $T_{\rm e}$. Similar observation is made in bulk InSb semiconductor whose optical phonon energy is 24.4 meV [46], closer to the one considered in the present work. In addition, $T_{\rm e}$ is found to have a strong (weak) dependence on $n_{\rm e}$ at low (large) E. The strong $n_{\rm e}$ dependence at low field may be attributed to the $n_{\rm e}$ dependence of $\mu_{\rm ap}$ and $P_{\rm ap}$. In figure 1(b), $T_{\rm e}$ vs E is shown for $n_{\rm e} = n_0$ for different $\tau_{\rm p}$. In the low field region, where ap scattering is dominant, $T_{\rm e}$ is independent of $\tau_{\rm p}$. The hot phonon effect is found to enhance $T_{\rm e}$, moderately, in the high field region. This is because, the number of hot phonons increases

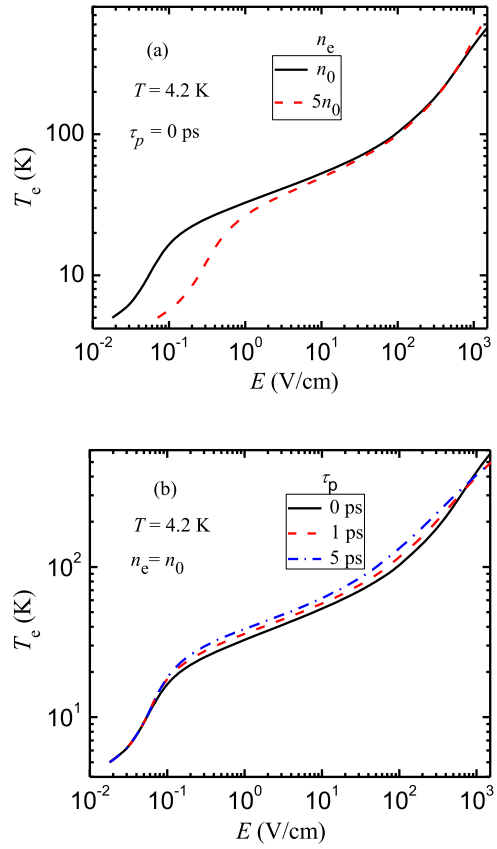

Figure 1. The electron temperature T_e as a function of electric field E, at $T = 4.2$ K. (a) For $n_e = n_0$ and $5n_0$ and $\tau_p = 0$ ps and (b) for $n_e = n_0$ and $\tau_p = 0$, 1 and 5 ps.

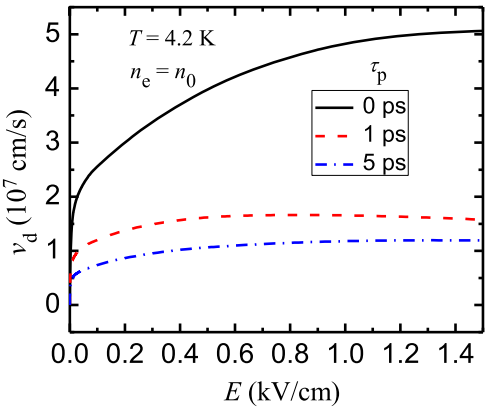

Figure 2. The electron drift velocity v_d as a function of electric field E, at $T = 4.2$ K, for electron density $n_e = n_0$ and phonon relaxation time $\tau_p = 0$, 1 and 5 ps.

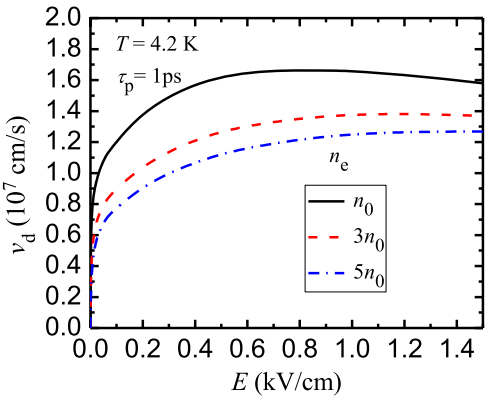

Figure 3. The electron drift velocity v_d as a function of electric field E, at $T = 4.2$ K, for electron densities $n_e = 1$, 3 and $5n_0$ and phonon relaxation time $\tau_p = 1$ ps.

with increasing T_e. This increased number of hot phonons can be described by the Bose distribution $N_{\mathbf{q}}(T_{ph})$, with effective hot phonon temperature T_{ph} being $T < T_{ph} < T_e$. The difference $T_e - T_{ph}$ decreases with increasing τ_p, and reduces the electron energy loss. Consequently, T_e is enhanced for larger τ_p.

In figure 2, the drift velocity v_d is plotted as a function of E, at $T = 4.2$ K, for $n_e = n_0$ and $\tau_p = 0$, 1 and 5 ps. The behavior is, as conventionally found, linear at very low field and becomes sub-linear for higher field. Finally, for further increase of E, v_d saturates or tends to saturate. This behavior is found to be the same for all τ_p. The saturation/ near saturation drift velocity has been found to be of the order of 10^7 cm s^{-1}. It is nearly the same as found in graphene [32, 34, 35], bulk silicon [47] and some of the 3D compound semiconductors [29]. The nonlinear behavior is generally attributed to the enhanced el–ph scattering with the increasing field. We may also explain the high field behavior using the energy and momentum balance equations. These equations imply that the drift velocity is given by P/Q. In order to understand the saturation/near saturation of v_d, we have to know the dependence of P and Q on T_e. At higher T_e (i.e. strong E), P has been found to increase rapidly with T_e [25], and hence with E. This is due to the enhanced scattering by optical phonons at high fields. Similar behavior is expected with Q. This rapid increase of momentum and energy loss rates results in saturation/near saturation of v_d.

The hot phonon effect can be captured, in figure 2, by comparing the v_d vs E curve of $\tau_p = 0$ ps with those of $\tau_p = 1$ and 5 ps. It is important to note that the effect of hot phonons is two-fold. It advances the saturation of v_d to occur at relatively low field $\sim 10^2$ V cm^{-1}. In addition, the hot phonon effect significantly degrades v_{ds}. For example, at $E = 1.5$ kV cm^{-1}, for $\tau_p = 0$, 1 and 5 ps, the v_{ds} are, respectively, found to be 5.0, 1.6 and 1.2 $\times$ 10^7 cm s^{-1}. The reduction in v_{ds} is by a factor of 3.1 (4.2) for $\tau_p = 1$ (5) ps. The degradation of v_d and v_{ds} may be attributed to the fact that the hot phonon population increases with increasing T_e [26] or E which increases scattering by phonons and results into reduction in v_d and v_{ds}. It is to be noted that the degradation of v_{ds} is also clearly seen in graphene [37].

With a view to see the effect of electron density on saturation velocity, the v_d vs E curves are presented in figure 3 for $n_e = n_0$, $3n_0$ and $5n_0$ taking $\tau_p = 1$ ps. It is found that v_d is smaller for larger n_e. However, the difference in magnitude is small.

We have examined the saturation velocity v_{ds} dependence on n_e, taken in range $1–10n_0$. The v_{ds} values are taken at $E = 1.5$ kV cm^{-1} for $T = 4.2$ K and $\tau_p = 1$ ps. The plot of v_{ds} as a function of n_e is shown in figure 4 for $\tau_p = 1$ ps. Expressing

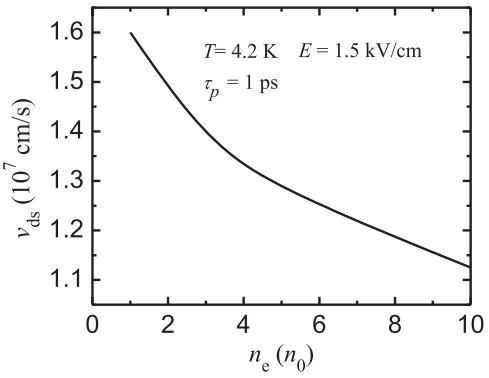

Figure 4. The electron saturation drift velocity v_{ds} as a function of electron density n_e, at $T = 4.2$ K and electric field $E = 1.5$ kV cm^{-1} for phonon relaxation time $\tau_p = 1$ ps.

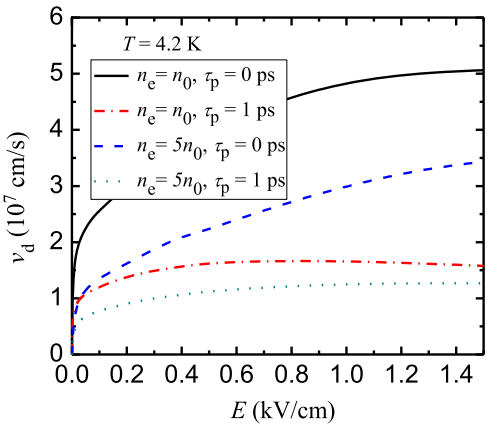

Figure 5. The electron drift velocity v_d as a function of electric field E, at $T = 4.2$ K, for electron density $n_e = 1$ and $5n_0$ and phonon relaxation time $\tau_p = 0$ and 1 ps.

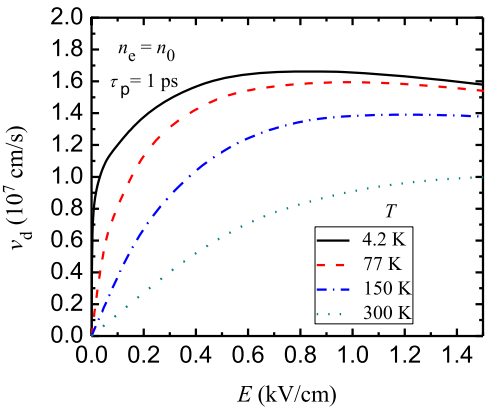

Figure 6. The electron drift velocity v_d as a function of electric field E, at $T = 4.2$, 77, 150 and 300 K for electron density $n_e = n_0$ and phonon relaxation time $\tau_p = 1$ ps.

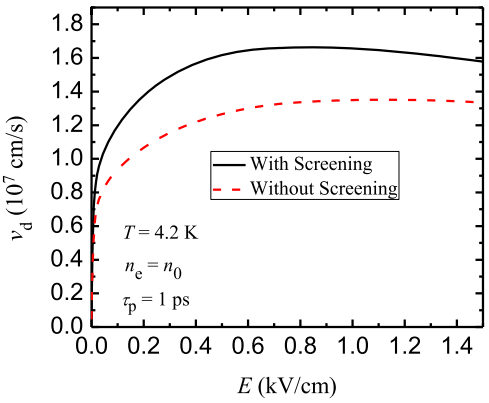

Figure 7. The electron drift velocity v_d as a function of electric field E, with and without screening, at $T = 4.2$ K, for $n_e = n_0$ and $\tau_p = 1$ ps.

$v_{ds} \alpha n_e{}^p$, we obtain $p = -0.2$. It indicates that v_{ds} has a weak dependence on n_e. Similar observation was made in graphene [32, 34, 36]. Moreover, we have also found that the effect of hot phonons, in degrading v_{ds}, is smaller for larger n_e (see figure 5). For example, at $E = 1.5$ kV cm^{-1}, for $\tau_p = 1$ ps, v_{ds} reduces by a factor of about 3.1 and 2.7, respectively, for $n_e = n_0$ and $5n_0$.

In order to analyze the effect of lattice temperature on the drift velocity, v_d vs E is depicted in figure 6 for lattice temperatures $T = 4.2$, 77, 150 and 300 K, with $n_e = n_0$ and $\tau_p = 1$ ps. All the curves exhibit the same behavior. For a chosen E, the v_d values are smaller for larger T. It may be attributed to the fact that, at larger T, more phonons are excited causing more scattering and reducing the v_d. At $E = 1.5$ kV cm^{-1}, the values of v_{ds} are about 1.6, 1.54, 1.38 and 1.00×10^7 cm s^{-1}, respectively, for $T = 4.2$, 77, 150 and 300 K. Besides, it is noticed that the saturation of v_d sets in at a higher field for larger T.

The effect of screening is brought out in figure 7, by plotting v_d as a function of E with and without screening of el–ph interaction. The curves are shown for $n_e = n_0$ and $\tau_p = 1$ ps at $T = 4.2$ K. It is found that, screening enhances v_d. This is expected as the screening effectively reduces the strength of el–ph coupling and hence the scattering of electrons. In the saturation region, screening is found to enhance v_d by about 20%.

In the following, we have discussed the current density dependence on E and n_e. In the literature [34, 35], Drude model, $j = n_e e v_d$ is used to study the current density. Accepting this model, the behavior of j as a function of E will be the same as that of v_d vs E. Then, saturation of current density also occurs at low fields of the order 10^2 V cm^{-1}. We have estimated saturation current density j_s using $j_s = n_e e v_{ds}$. For $n_e = 1 \times 10^{18}$ cm^{-3} and $\tau_p = 1$ ps, the v_{ds} is about 1.6×10^7 cm s^{-1} at $E = 1.5$ kV cm^{-1}. Then, at this value of E, we get a large saturation current density $j_s = 2.56 \times 10^6$ A cm^{-2}. This is about 3 orders of magnitude greater than that found in conventional 3D semiconductors [29]. The n_e dependence of j_s can be expressed as $j_s \sim n_e{}^{p+1}$. With p nearly equal to -0.2, j_s increases almost linearly with increasing n_e. In graphene also, j_s has exhibited the same electron density dependence [34]. The large value of j_s in 3DDS Cd_3As_2 is because of the large n_e, which is about 2–3 orders of magnitude greater than that in the conventional 3D semiconductors [29]. In graphene, j_s is few tens of A cm^{-1} [36, 37].

We would like to point out that, at high bias, the current density is usually described by the 'saturated current density model' $j = n_e e\mu E/\{1 + (\mu E/v_{ds})\}$ [36], which is modification of Drude model. Then, the current density, in the high field region, estimated using this relation, is smaller by a factor $r = \{1 + (\mu E/v_{ds})\}$ than the one estimated from Drude model. In the saturation region, $r = 2$. Even with this model, j_s will be of the order of 10^6 A cm^{-2}.

The degradation of v_{ds}, due to the hot phonon effect, can be inhibited by reducing the phonon relaxation time τ_p. In graphene, it has been shown that the hot phonon effect can be diminished by 'isotopic disorder engineering' and there by v_{ds} can be enhanced [37]. This has been achieved by introducing isotropic disorder in the sample.

We point out that, while disorder/impurity scattering determines the low field mobility at low temperature [21, 22], the saturation of v_d has been attributed to the scattering by optical phonons. Consequently, the saturation of velocity and hence the current density are apparently not affected by impurity in nearly intrinsic samples with very small residual resistivity $\sim$ 10 nΩ cm [8, 10]. The n_e in intrinsic/nearly intrinsic samples might be due to unintentional background impurities. The density of such impurities could be different in different samples and varying in an unknown manner. However, in samples with residual resistivity $\sim$ 10 $\mu\Omega$ cm [9, 16–18], v_d may degrade due to impurity scattering, even in saturation region, but marginally as found in graphene [35]. The effect of impurity scattering can be taken in to account in our calculation by taking the resultant hot electron mobility as $\mu = [(1/\mu_{ap}) + (1/\mu_{op}) + (1/\mu_{im})]^{-1}$, where μ_{im} is the hot electron mobility due to impurity scattering. In graphene, it is also found that as sample quality improves the saturation will occur at lower field [35].

In graphene, it has been shown that larger the acoustic deformation potential coupling constant D, larger is the v_d and v_{ds} [32]. This is because, scattering by acoustic phonons is dominant up to $\sim$200 K as the optical phonon scattering becomes important above this temperature due to the large optical phonon energy ($\sim$190 meV). In Dirac semimetal Cd_3As_2, a variation of D may affect v_{ds} to a small extent as the optical phonon scattering becomes dominant for temperatures $> \sim$40–50 K [22] and the saturation of drift velocity occurs at relatively higher temperature.

Although the predicted current density in the present work is very large, while applying 3DDS Cd_3As_2 in FETs, it is required to address the off current density, as on/off ratio of the current is important. It is possible that, due to zero band gap, the intrinsic (thermally generated) carrier density could be large, as in bulk gapless semiconductors HgTe [48] and HgSe [49], which may lead to a large off current density and reduced on/off current ratio. The room temperature on/off current ratio is 4 in zero gap monolayer graphene, and about 100 in finite gap bilayer graphene [50]. The problem of large off current density may be overcome in Cd_3As_2 by creating a band gap by some means, for e.g. by forming a film of few tens of nm thickness [27].

We would like to remark that, in the present investigation, el–op interaction via Fröhlich coupling with one optical phonon branch of energy 25 meV is considered, although there can be numerous optical branches. A good discussion of this choice is given in our earlier work [22]. This is also evinced in the phonon mediated hot electron cooling of photoexcited carriers via pump-probe measurements [38].

4. Summary

Theoretically, the drift velocity v_d dependence on electric field E is investigated in an intrinsic three-dimensional Dirac semimetal Cd_3As_2. The hot electron mobility and energy balance equations are obtained, considering the electron scattering by acoustic and optical phonons with the screened interactions. The saturation velocity $v_{ds} \sim 10^7$ cm s^{-1} has been found at relatively small electric field ($\sim 10^2$ V cm^{-1}). The effects of hot phonons and electron density n_e on v_d and v_{ds} are explored. The hot phonon effect has a strong impact on v_{ds}. It sets in the saturation velocity at low electric field and significantly degrades v_{ds}. Furthermore, v_{ds} has a weak dependence on electron density. The effect of screening is found to enhance v_d moderately. A saturation current density $j_s \sim 10^6$ A cm^{-2} is predicted. This large j_s is attributed to the large v_{ds} and n_e in this material. In addition, in the process of developing hot electron mobility, we have obtained the power laws for T_e and n_e dependence of μ in the Bloch–Grüneisen and equipartition regimes. Our theoretical predictions may be tested as and when the experimental results are available.

ORCID iDs

S S Kubakaddi https://orcid.org/0000-0002-4702-868X

References

[1] Armitage N P, Mele E J and Vishwanath A 2018 *Rev. Mod. Phys.* **90** 015001
[2] Crassee I, Sankar R, Lee W-L, Akrap A and Orlita M 2018 *Phys. Rev. Mater.* **2** 120302
[3] Wang Z, Weng H, Wu Q, Dai X and Fang Z 2013 *Phys. Rev.* B **88** 125427
[4] Borisenko S, Gibson Q, Evtushinsky D, Zabolotnyy V, Büchner B and Cava R J 2014 *Phys. Rev. Lett.* **113** 027603
[5] Liu Z K *et al* 2014 *Nat. Mater.* **13** 677
[6] Jeon S *et al* 2014 *Nat. Mater.* **13** 851
[7] Neupane M *et al* 2014 *Nat. Commun.* **5** 3786
[8] Liang T, Quinn G, Ali Mazhar N, Liu M, Cava R J and Ong N P 2015 *Nat. Mater.* **14** 280
[9] He L P, Hong X C, Dong J K, Pan J, Zhang Z, Zhang J and Li S Y 2014 *Phys. Rev. Lett.* **113** 246402
[10] Zhao Y *et al* 2015 *Phys. Rev.* X **5** 031037
[11] Feng J *et al* 2015 *Phys. Rev.* B **92** 081306
[12] Narayanan A *et al* 2015 *Phys. Rev. Lett.* **114** 117201
[13] Schumann T, Galletti L, Kealhofer D A, Kim H, Goyal M and Stemmer S 2018 *Phys. Rev. Lett.* **120** 016801
[14] Goyal M, Galletti L, Salmani-Rezaie S, Schumann T, Kealhofer D A and Stemmer S 2018 *APL Mater.* **6** 026105
[15] Li H, He H, Lu H Z, Zhang H, Liu H, Ma R, Fan Z, Shen S Q and Wang J 2016 *Nat. Commun.* **7** 10301
[16] Zhang Y, Zhang C, Gao H, Liu Y, Liu X, Xiu F and Kou X 2018 *Appl. Phys. Lett.* **113** 072104

[17] Wang H *et al* 2019 *Adv. Funct. Mater.* **29** 1902437
[18] Pariari A, Khan N, Singha R, Satpati B and Mandal P 2016 *Phys. Rev.* B **94** 165139
[19] Zhou T, Zhang C, Zhang H, Xiu F and Yang Z 2016 *Inorg. Chem. Front.* **3** 1637
[20] Lundgren R, Laurell P and Fiete G A 2014 *Phys. Rev.* B **90** 165115
[21] Das Sarma S, Hwang E H and Min H 2015 *Phys. Rev.* B **91** 035201
[22] Kubakaddi S S 2019 *J. Appl. Phys.* **126** 135703
[23] Lundgren R and Fiete G A 2015 *Phys. Rev.* B **92** 125139
[24] Bhargavi K S and Kubakaddi S S 2016 *Phys. Status Solidi* **10** 248
[25] Kubakaddi S S and Biswas T 2018 *J. Phys.: Condens. Matter* **30** 265303
[26] Galletti L, Schumann T, Shoron O F, Goyal M, Kealhofer D A, Kim H and Stemmer S 2018 *Phys. Rev.* B **97** 115132
[27] Shoron O F, Schumann T, Goyal M, Kealhofer D A and Stemmer S 2019 *Appl. Phys. Lett.* **115** 062101
[28] Conwell E M 1967 *High Field Transport in Semiconductors* (New York: Academic)
[29] Nag B R 1980 *Electron Transport in Compound Semiconductors* (Springer Series in Solid State Sciences) (Berlin: Springer) vol 11 p 311
[30] Ferry D K 1991 *Semiconductors* (New York: Macmillan) p 321
[31] Ridley B K 1991 *Rep. Prog. Phys.* **54** 169
[32] Shishir R S and Ferry D K 2009 *J. Phys.: Condens. Matter.* **21** 344201
Ferry D K 2016 *Semicond. Sci. Technol.* **31** 11LT02
[33] Bao W S, Liu S Y, Lei X L and Wang C M 2009 *J. Phys.: Condens. Matter* **21** 305302
[34] Bistritzer R and MacDonald A H 2009 *Phys. Rev.* B **80** 085109
[35] DaSilva A M, Zou K, Jain J K and Zhu J 2010 *Phys. Rev. Lett.* **104** 236601
[36] Perebeinos V and Avouris P 2010 *Phys. Rev.* B **81** 195442
[37] Fang T, Konar A, Xing H and Jena D 2011 *Phys. Rev.* B **84** 125450
[38] Lu W *et al* 2017 *Phys. Rev.* B **95** 024303
[39] Ridley B K 1999 *Quantum Processes in Semiconductors* 4th edn (Oxford: Oxford Science Publications, Clarendon Press) p 318
[40] Ridley B K 1989 *Semicond. Sci. Technol.* **4** 1142
[41] Bhargavi K S and Kubakaddi S S 2014 *Physica* E **56** 123
[42] Cao J *et al* 2015 *Nat. Commun.* **6** 7779
[43] Jay-Gerin J P, Aubin M J and Caron L G 1978 *Phys. Rev.* B **18** 4542
[44] Kampfrath T, Perfetti L, Schapper F, Frischkorn C and Wolf M 2005 *Phys. Rev. Lett.* **95** 187403
[45] Tse W-K and Das Sarma S 2009 *Phys. Rev.* B **79** 235406
[46] Shimomae K, Hirose Y and Hamaguchi C 1981 *J. Phys. C: Solid State Phys.* **14** 5151
[47] Jacoboni C, Canali C, Ottaviani G and Alberigi Quaranta A 1977 *Solid State Electron.* **20** 77
[48] Guldner Y, Rigaux C, Grynberg M and Mycielski A 1973 *Phys. Rev.* B **8** 3875
[49] Lehoczky S L, Broerman J G, Nelson D A and Whitsett C R 1974 *Phys. Rev.* B **9** 1598
[50] Xia F, Farmer D B, Lin Y and Avouris P 2010 *Nano Lett.* **10** 715